Alteration of citrine structure by hydrostatic pressure explains the accompanying spectral shift

Buz Barstow*, Nozomi Ando[†‡], Chae Un Kim[‡§], and Sol M. Gruner*[†§¶]

*School of Applied Physics, [†]Department of Physics, and [§]Cornell High Energy Synchrotron Source, Cornell University, Ithaca, NY 14853

Edited by Roland Winter, Dortmund University of Technology, Dortmund, Germany, and accepted by the Editorial Board June 4, 2008 (received for review March 6, 2008)

A protein molecule is an intricate system whose function is highly sensitive to small external perturbations. However, no examples that correlate protein function with progressive subangstrom structural perturbations have thus far been presented. To elucidate this relationship, we have investigated a fluorescent protein, citrine, as a model system under high-pressure perturbation. The protein has been compressed to produce deformations of its chromophore by applying a high-pressure cryocooling technique. A closely spaced series of x-ray crystallographic structures reveals that the chromophore undergoes a progressive deformation of up to 0.8 Å at an applied pressure of 500 MPa. It is experimentally demonstrated that the structural motion is directly correlated with the progressive fluorescence shift of citrine from yellow to green under these conditions. This protein is therefore highly sensitive to subangstrom deformations and its function must be understood at the subangstrom level. These results have significant implications for protein function prediction and biomolecule design and engineering, because they suggest methods to tune protein function by modification of the protein scaffold.

fluorescence | high-pressure x-ray crystallography | protein engineering | protein structure-function | yellow fluorescent protein

It is well known that the three-dimensional structure of a protein molecule is crucial to understanding its function (1). Because protein molecules have dimensions of tens to hundreds of angstroms, subangstrom positional perturbations may naïvely appear insignificant (2). However, if one considers two objects interacting through a Lennard–Jones potential that are separated by 3.5 Å and moves them together by just 0.1 Å, the potential energy between these objects will change by $(1/3.4^6)/(1/3.5^6) = 1.19$, or 19%. This calculation suggests that changes as small as 0.1 Å in the relative positions of critical functional groups could make a large difference in the energy of an electronic transition and thus a notable change in protein function (3).

The sensitivity of protein function to subangstrom positioning of critical functional groups is implied by the observation that modest pressures (less than a few hundred MPa) significantly modify protein function (4). For example, the flash decay rate of firefly luciferase is reduced (5), the oxygen binding affinity of human hemoglobin is doubled (6), and oxidation rates by morphinone reductase are increased (7). Protein atomic structures at up to a few hundred MPa (8–16) indicate that atoms in protein molecules are typically displaced by ≈0.1–1.0 Å from their ambient pressure positions. These observations suggest that the exact positioning of atoms, especially in the active sites of catalytic proteins, is an important feature of protein operation and that this positioning is subject to environmental perturbation.

To systematically investigate the correlation between protein function and small structural deformations, we selected the *Aequorea* Yellow Fluorescent Protein (YFP) citrine (17–19), an extremely bright, intrinsically fluorescent protein whose atomic structure is known to 2.2-Å resolution (17), which displays a fluorescence peak shift of ≈1 nm/100 MPa at room temperature [supporting information (SI) *Text* and Fig. S1] (20).

The most notable feature of the YFP family is the stacking of a phenol ring, the side chain of tyrosine 203, 3.4 Å above the main chromophore found in all *Aequorea* fluorescent proteins. The weak interaction of the main chromophore and the tyrosine 203 phenol is speculated to be responsible for shifting the fluorescence peak of citrine from green to yellow (18). A diagram of citrine and its chromophore is shown in Fig. 1. One can imagine that a small pressure-induced deformation of the β-barrel scaffold of citrine could perturb the relative positions of the main chromophore and tyrosine 203, changing their weak interaction, and alter the fluorescence properties of citrine.

Results

A closely spaced series of structures of citrine was solved by using a high-pressure x-ray crystallography technique developed by Kim *et al.* (9). A protein crystal is pressurized with helium gas and is then cooled to 77 K, locking in collective pressure-induced structural changes (8–9). After pressure release, the protein molecules composing the crystal will retain many of the collective changes of the pressurized state, on the condition that the crystal's temperature remains well below its glass transition temperature (4, 8, 21). Citrine crystals were prepared at pressures ranging from 50 to 500 MPa. In total, data from 30 high-quality crystals was condensed into 26 atomic models by using a standardized refinement procedure (*SI Text*). Each structure at every pressure is derived from a different crystal at cryogenic temperatures. The high-resolution limit of the datasets ranged from 1.5 to 2.46 Å (*SI Text*), typically <2 Å.

Subangstrom structural shifts also occur upon cooling to cryogenic temperatures (8, 22), complicating pressure cryocooling analysis. To establish a direct link to the high-pressure cryocooled structures of citrine, fluorescence spectra of high-pressure cryocooled citrine samples were measured with a crystal spectrophotometer (23–24) (*SI Text*). Optimal spectra were obtained from dilute solutions of citrine in optically clear polycarbonate capillaries with well defined path lengths (25) (*SI Text*). Solutions were prepared with absorbances <0.1 while maintaining strong fluorescence with a satisfactory signal to background and high-pressure cryocooled. Background subtraction was performed with a high-pressure cryocooled reference at each pressure level. The fluorescence peak of citrine solutions shifts from 527 nm when frozen at ambient pressure to 530 nm

Author contributions: B.B., N.A., C.U.K., and S.M.G. designed research; B.B., N.A., and C.U.K. performed research; B.B., N.A., C.U.K., and S.M.G. analyzed data; and B.B., N.A., and S.M.G. wrote the paper.

The authors declare no conflict of interest.

This article is a PNAS Direct Submission. R.W. is a guest editor invited by the Editorial Board.

Data deposition: The atomic coordinates have been deposited in the Protein Data Base, www.pdb.org (accession codes are listed in Table S5).

[‡]N.A. and C.U.K. contributed equally to this work.

[¶]To whom correspondence should be addressed at: 162 Clark Hall, Cornell University, Ithaca, NY 14853. E-mail: smg26@cornell.edu.

This article contains supporting information online at www.pnas.org/cgi/content/full/0802252105/DCSupplemental.

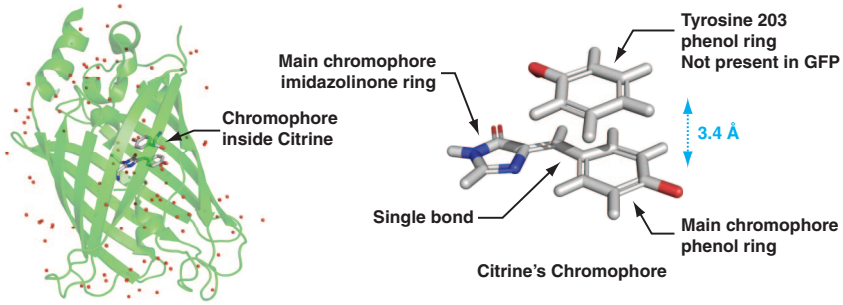

Fig. 1. The citrine molecule and citrine's chromophore.

at 50 MPa and to 510 nm at 360 MPa, with most of the shift occurring by 250 MPa (Fig. 2*A*).

The fluorescence peak shift from yellow to green suggests that the perturbing interaction of tyrosine 203 is slowly removed by the application of high-pressure. The fluorescence peak shift of pressure cryocooled citrine relaxes to yellow upon warming of the sample above a critical temperature (≈180 K). It does not return to its original position upon recooling, suggesting that the original fluorescence shift to the green had been locked in by the high-pressure cryocooling procedure. The fluorescence peak of a high-pressure cryocooled solution that was slowly warmed and recooled is shown as a function of temperature in Fig. 2 *B* and *C*. This relaxation effect is also observed in citrine crystals at approximately the same temperature (*SI Text* and Fig. S2). The fluorescence peak of monomeric EGFP, which lacks the perturbing tyrosine 203 ring, does not shift as a function of pressure.

To reduce possible random and systematic coordinate errors in the high-pressure cryocooled structures of citrine, multiple models were constructed at different pressure levels, using data from a new crystal for each model. This procedure allowed the calculation of an average and standard deviation for each atomic coordinate. The standard deviations were compared with the approximate coordinate estimate error by Cruickshank (26) and found to be less than or equal to this estimate. The construction of multiple models at each pressure level permits the identification of structural deformations below the resolution limit of any individual dataset.

The crystal structures of high-pressure cryocooled citrine reveal a small but progressive reorientation of the two stacked aromatic rings that compose citrine's chromophore. This deformation of the chromophore smoothly increases with pressure and stands out from atomic coordinate error. Structures of the main chromophore and tyrosine 203 of the highest quality structures at representative pressures are shown in Fig. 3. The tyrosine 203 phenol rings of the high-pressure cryocooled structures were aligned by using the LSQKAB program (27) to allow inspection of the main chromophore position relative to tyrosine 203. This aligned tyrosine 203 coordinate system is also defined in Fig. 3. The origin of the aligned tyrosine 203 coordinate system is at the center of the tyrosine 203 phenol ring. The x and y axes of this system are embedded in the plane of the phenol ring, whereas the z axis is normal to this plane. The x, y, and z axes are oriented so that all motions with increasing pressure have a positive sign.

Plots of the motion of the main chromophore's two rings in the aligned tyrosine 203 coordinate system are shown in Fig. 4. The center of the main chromophore's phenol ring slides underneath the stacked tyrosine 203 phenol with increasing pressure. This sliding motion is confined to a plane parallel to the x-y plane and 3.4 Å below it, at $z \approx -3.4$ Å. The maximum extent of the swing is ≈0.8 Å over 500 MPa. The largest component of motion is approximately +0.5 Å in the y-direction, moving the main chromophore away from the origin. The motion in the x-direction brings the center of the main chromophore's phenol ≈0.4 Å closer to the origin of the coordinate system. The center of mass of the main chromophore's imidazolinone ring moves by 0.5 Å in y, 0.4 Å in x, and 0.2 Å in z (Fig. 4).

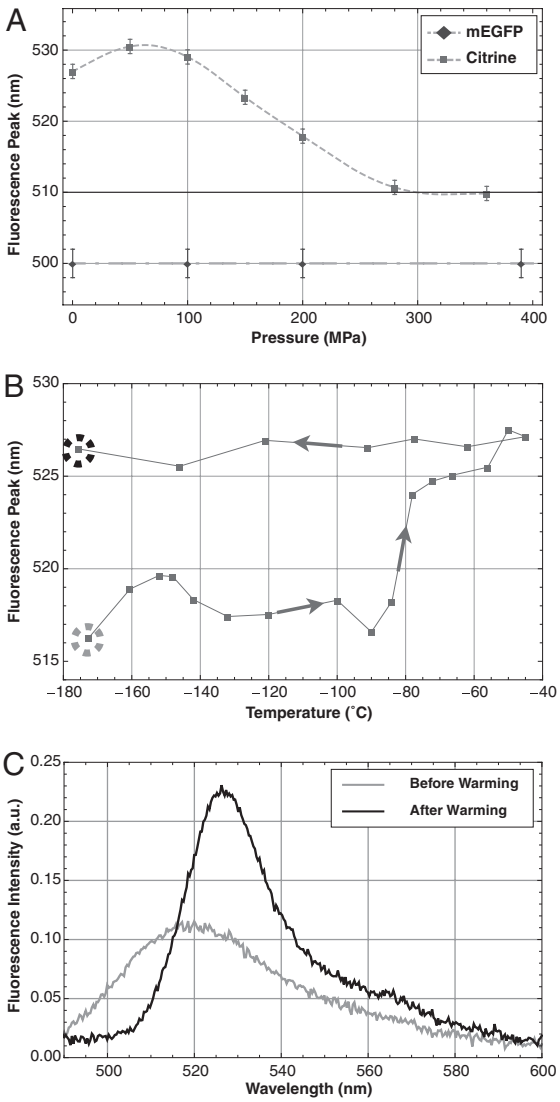

Fig. 2. Pressure-induced fluorescence peak shift of citrine. (*A*) Citrine's fluorescence peak under high-pressure cryocooling (squares), with connecting line to aid eye, and mEGFP's fluorescence peak under identical conditions (diamonds). Fit is shown as a dashed line. (*B*) Fluorescence peak of citrine solution in capillary pressurized to 200 MPa as it is warmed. Note dashed circles surrounding start (gray) and end (black) points of curve, corresponding to spectra of high-pressure cryocooled citrine solution before and after warming, as shown in *C*.

BIOPHYSICS

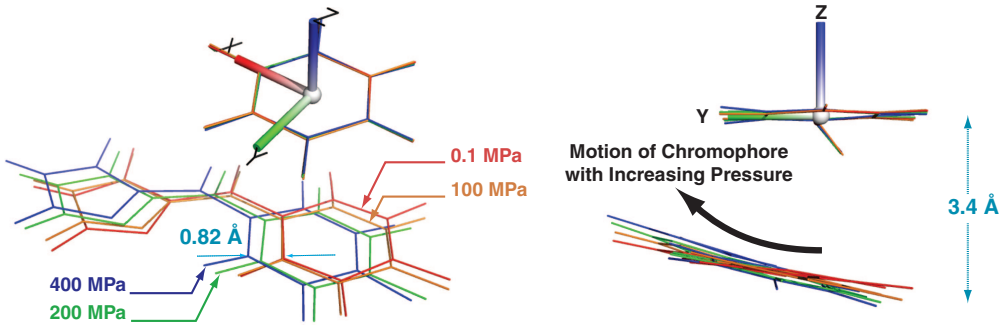

Fig. 3. X-ray crystal structures of citrine's chromophore at selected pressures with the lowest R_{Free} factors. Note the *x-y-z* coordinate axes defined in this figure. The origin of the coordinate system is at the center of the tyrosine 203 phenol ring. Note that the centers of mass of the main chromophore phenol and imidazolinone rings have negative *z* coordinates.

In addition to sliding, the main chromophore phenol ring reorients with respect to the tyrosine 203 phenol ring and the main chromophore's imidazolinone ring. The normal vector to the main chromophore's phenol ring rotates from 7°, with respect to the *z*-axis, to 14°, by 500 MPa (Fig. 4). The normal to the main chromophore imidazolinone ring rotates by <5°, changing the orientation of the two rings composing the main chromophore (Fig. 4).

The progressive deformation of citrine's structure under high-pressure cryocooling reveals a mechanism for the shift toward the green of citrine's fluorescence peak. The relative positions of the main chromophore and the perturbing tyrosine 203 phenol ring separate with increasing pressure, removing the perturbing influence of the tyrosine 203 phenol and allowing the main chromophore to return to its unperturbed, green fluorescent state. The removal of the perturbing interaction requires a structural shift of only 0.8 Å.

Discussion

We have demonstrated that small deformations of only several tenths of one angstrom in the active site of the YFP molecule citrine, induced by high-pressure cryocooling, can measurably affect its function: fluorescence. This deformation shifts the fluorescence peak of the molecule from yellow to green.

To interpret the relationship between the positions of the main chromophore and tyrosine 203 (Fig. 4) and the fluorescence peak of citrine (Fig. 2), we must consider the degree of alignment of the two rings. The overlap of the tyrosine 203 phenol with the

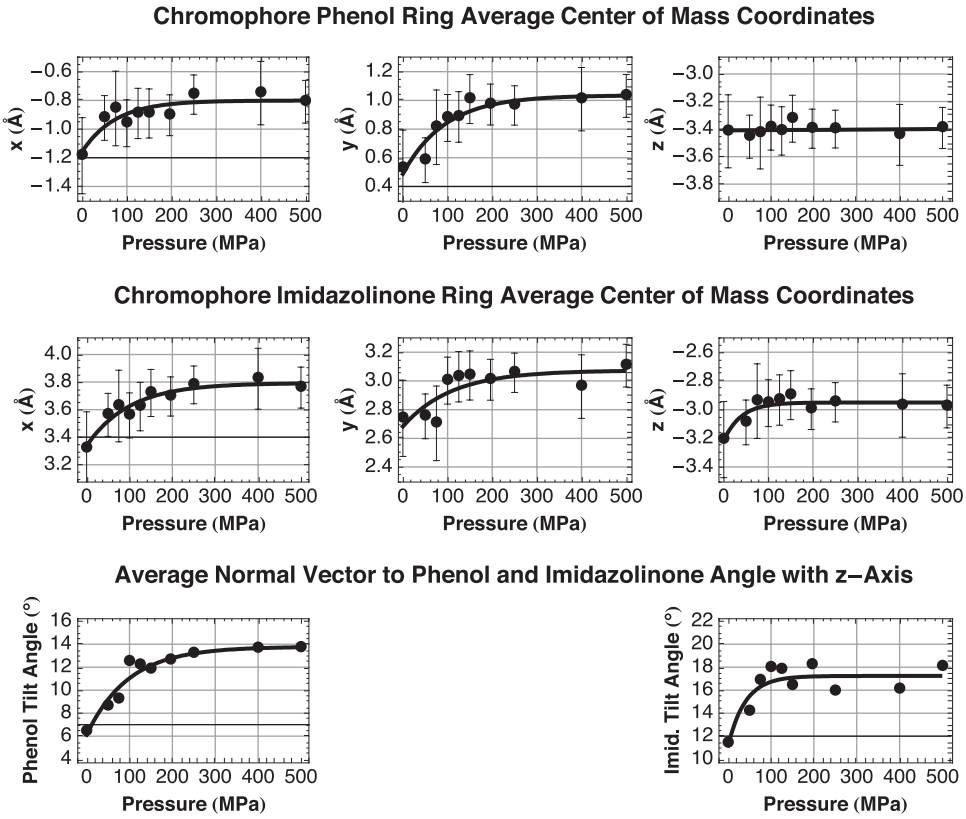

Fig. 4. Average center of mass positions of the main chromophore phenol and imidazolinone rings in the coordinate system defined in Fig. 3. Error bars were estimated by Cruickshank's formula. Fits are shown as solid gray lines.

main chromophore shifts the fluorescence peak toward yellow under ambient conditions (18). There are two notable pressure regions in Fig. 2*A*, one at pressures >100 MPa and another at ≈50 MPa. We showed that at pressures exceeding 100 MPa, the tyrosine 203 phenol is pushed far enough away from the main chromophore to blue-shift the spectrum of citrine to the green. This results in a spectrum that is more like EGFP, with a fluorescence peak at 510 nm (19). At ≈50 MPa, there is a small red-shift of the fluorescence peak. This red-shift is interesting, because it demonstrates that, under ambient conditions, the perturbing influence of the tyrosine 203 phenol on the main chromophore is not maximized. The application of a small pressure, ≈50 MPa, is enough to increase the perturbation on the main chromophore.

As noted earlier, the function of many proteins is strongly affected by pressure, yet they are highly incompressible, only one-twentieth to one-third as compressible as water (28). The effect of pressure is not to isotropically compress the molecule, but to alter its ensemble of allowed conformations. Many specific interactions may be involved, including changes in hydration and ionization of surface groups and reduction of void volume. As a protein is a system of linked parts, small pressure-induced structural changes across the molecule may be communicated to the active site, resulting in functional changes, which appears to be the case with citrine: The deformation of the β-barrel scaffold is communicated to the aromatic rings directly involved in fluorescence.

Dietz *et al.* (29–31) have performed single molecule unfolding experiments on GFP molecules by using optical tweezers. One speculates that a similar experiment could be performed where mechanical forces, such as those produced by the tip of an atomic force microscope (AFM) or optical tweezers, could be used to distort the protein to see whether it results in a similar spectral shift. The global effect of pressure on the citrine β-barrel structure is that the barrel bends slightly to one side (data not shown). This deformation is communicated to the chromophore. It would be of interest to mechanically bend the barrel to one side by pushing on it with the AFM tip to see whether the spectrum shifts. Although this would be a very difficult experiment to perform, it is in principle feasible.

The pressure dependent behavior of citrine provides a test of models of protein fluorescence (32–33). This type of simultaneous study of the activity and structure of protein molecules under progressive deformation will provide challenging tests for, and may allow the improvement of, many computer models of protein function. An improvement in protein function prediction algorithms may have important benefits for rational protein design. It is likely that small (<1 Å) structural deformations in the active sites of many proteins may have measurable effects on their functions. It is also possible that seemingly small refinement errors (on the order of 0.1 Å) in atomic structures of proteins, derived from low-resolution data or by homology modeling of known structures, could lead to substantial errors on the predicted catalytic activities of these proteins (34). These results also suggest that, to achieve maximum efficiency in their design goal, designed macromolecules may need to be engineered with subangstrom structural accuracy. High-pressure perturbation may provide a means to explore catalytic rate enhancement, and to achieve it, by suggesting sites at which strain-inducing mutations (35) may be introduced into the protein scaffold to mimic the effects of high-pressure under ambient conditions that would not be highlighted by other methods.

Materials and Methods

Protein Expression, Purification, and Crystallization. The gene for citrine was kindly provided by R. Y. Tsien (University of California at San Diego) in a pRSETB (Invitrogen) plasmid. The gene was extracted from the plasmid by PCR, the N-terminal enterokinase cut site was replaced by a Tobacco Etch Virus (TEV) protease cut site, and the resulting gene was ligated into a pET28 plasmid (Novagen). Citrine was expressed in *E. coli* strain BL21 and was purified by affinity chromatography. Polyhistidine affinity tags were digested by the TEV protease and removed by affinity chromatography using a Ni-NTA column (HisTrap HP, catalog number 17-5248-01, GE Healthcare). Gel filtration was performed as a final purification step. Citrine was stored in 50 mM HEPES (pH 7.5) and concentrated to 20 mg/ml with a centrifugal concentrator (catalog number OD010C37, Pall Separation Systems).

A citrine crystal was initially grown at 9% wt/vol PEG 3350 (catalog number HR2-591, Hampton Research) in 50 mM sodium acetate and 50 mM ammonium acetate, at pH 4.5 and 4°C. This crystal was used to produce a seed stock from which further crystals were grown (Fig. S3). Later citrine crystals were produced by using a Seed Bead (Hampton Research) to produce a seeded 1:1 mixture of 5% wt/vol PEG 3350, 50 mM sodium acetate, and 50 mM ammonium acetate (pH 5.0). Ten-microliter droplets of this mixture were dispensed onto glass cover-slides and sealed over wells containing a 5% wt/vol PEG 3350, 50 mM sodium acetate, and 50 mM ammonium acetate (pH 5.0) precipitant solution, in a hanging droplet configuration. Complete details can be found in *SI Text*.

Data Collection and Macromolecular Refinement. X-ray diffraction data were collected from high-pressure cryocooled citrine crystals at Cornell High Energy Synchrotron Source Station F2. Crystals were transferred by hand to the station goniometer and cryogenic nitrogen cold stream. Typically, 120–180 oscillation images were taken from each crystal, with an angular separation of 1°, a 1° oscillation angle, and exposure times from 30 to 60 seconds. Full data collection details are shown in Table S1. The diffraction data were indexed with Rossmann and van Beek's (36) Data Processing Suite algorithm, integrated with MOSFLM, scaled with Scala (37) and truncated with Truncate (38). Indexing quality indicators for each structure are shown in Table S2. Unit cell axes for each model are shown in Table S3. A full description of data collection can be found in *SI Text*. Model refinement was standardized for all models. Molecular replacement was performed with Molrep (39), followed by rigid body refinement, restrained refinement with an overall B-factor, and restrained refinement with an isotropic B-factor by refmac5 (40). Alternating cycles of solvent addition and restrained refinement were performed with ARP/wARP (41) and refmac5. Finally, the structures were validated with Coot (42) and PROCHECK (43). Full details of the crystallographic refinement procedure, quality indicators for all datasets, and the PDB accession codes can be found in *SI Text* and Tables S4–S5. Protein graphics were prepared with PyMOL (DeLano Scientific).

Low Temperature Spectroscopy. A fiber-fed, backscattering spectrophotometer, based upon designs by Hadfield and Hajdu (23) and Klink *et al.* (24), was constructed to measure the fluorescence spectra of high-pressure cryocooled citrine solution samples. Samples were contained in polycarbonate capillaries (914.4 μm outer diameter, 304.8 μm inner diameter, plastic part number 8-000-1000, Drummond Scientific) and excited with a 473-nm diode laser (catalog number LRS-473-TM-10, LaserGlow). Spectra were recorded with a USB2000 spectrophotometer (Ocean Optics). The sample temperature was controlled with a cryogenic nitrogen stream (Molecular Structure). Complete details are available in *SI Text*.

ACKNOWLEDGMENTS. We thank Dr. Cynthia Kinsland and the staff of the Cornell Life Sciences Core Lab Center's Protein Facility for assistance with the modification and expression of citrine vectors and protein purification; Professors Roald Hoffmann and Jason D'Acchioli for invaluable assistance in quantum chemistry; the MacCHESS staff at the Cornell High Energy Synchrotron Source (CHESS) for assistance in data collection and reduction; Martin Novak for invaluable assistance with the construction of experiments; Yi-Fan Chen and Dr. Mark Tate for the construction of the internals of the high-pressure cryocooling apparatus; Odin Wojcik and AccuFab, Inc., for the construction of the high-pressure cryocooling safety enclosure; Professor Warren Zipfel for providing a sample of monomeric EGFP; Professor Roger Tsien for providing the citrine plasmid; Dr. Ismail Hafez and Professors Lois Pollack, Brian Crane, and John Marohn for useful discussions; Professor Robert Campbell for assistance with crystallization of citrine; Elizabeth Landrum and Darren Southworth for assistance in data collection; and Joan Lenz and Dr. Raymond Molloy for assistance with molecular biology. This work is supported by Department of Energy Office of Biological and Envrionmental Research Grant FG02-97ER62443 and National Institutes of Health Protein Structure Initiative Grant GM074899. CHESS is supported by the National Institutes of Health via National Science Foundation Award DMR-0225180, and MacCHESS is supported by National Institutes of Health Grant RR001646.

1. Perutz MF, Fermi G, Luisi B, Shaanan B, Liddington RC (1987) Stereochemistry of cooperative mechanisms in hemoglobin. *Acc Chem Res* 20:309–321.
2. Daopin S, Davies DR, Schlunegger MP, Grütter MG (1994) Comparison of two crystal structures of TGF-β2: The accuracy of refined protein structures. *Acta Crystallogr D* 50:85–92.
3. Suydam IT, Snow CD, Pande VS, Boxer SG (2006) Electric fields at the active site of an enzyme: Direct comparison of experiment with theory. *Science* 313(5784):200–204.
4. Frauenfelder H, *et al.* (1990) Proteins and pressure. *J Phys Chem* 94:1024–1037.
5. Ueda I, Minami H, Matsuki H, Inoue T (1999) Does pressure antagonize anesthesia? High-pressure stopped-flow study of firefly Luciferase and anatomy of initial flash. *Biophys J* 76:478–482.
6. Carey FG (1977) Effect of hydrostatic pressure on ligand binding to hemoglobin. *J Biol Chem* 252:4102–4107.
7. Hay S, Sutcliffe MJ, Scrutton NS (2007) Promoting motions in enzyme catalysis probed by pressure studies of kinetic isotope effects. *Proc Natl Acad Sci USA* 104:507–512.
8. Urayama P, Phillips GN, Gruner SM (2002) Probing substates in sperm whale myoglobin using high-pressure crystallography. *Structure* 10:51–60.
9. Kim CU, Kapfer R, Gruner SM (2005) High-pressure cooling of protein crystals without cryoprotectants. *Acta Crystallogr D* 61:881–890.
10. Kundrot CE, Richards FM (1986) Collection and processing of x-ray diffraction data from protein crystals at high pressure. *J Appl Crystallogr* 19:208–213.
11. Kundrot CE, Richards FM (1987) Crystal structure of hen egg-white lysozyme at a hydrostatic pressure of 1000 atmospheres. *J Mol Biol* 193:157–170.
12. Fourme R., *et al.* (2001) High-pressure protein crystallography (HPPX): Instrumentation, methodology and results on lysozyme crystals. *J Synchrotron Radiat* 8(Pt 5):1149–1156.
13. Refaee M, Tezuka T, Akasaka K, Williamson MP (2003) Pressure-dependent changes in the solution structure of hen egg-white lysozyme. *J Mol Biol* 327:857–865.
14. Williamson MP, Akasaka K, Refaee M (2003) The solution structure of bovine pancreatic trypsin inhibitor at high pressure. *Protein Sci* 12:1971–1979.
15. Collins MD, Hummer G, Quillin ML, Matthews BW, Gruner SM (2005) Cooperative water filling of a nonpolar protein cavity observed by high-pressure crystallography and simulation. *Proc Natl Acad Sci USA* 102:16668–16671.
16. Collins MD, Quillin ML, Hummer G, Matthews BW, Gruner SM (2007) Structural rigidity of a large cavity-containing protein revealed by high-pressure crystallography. *J Mol Biol* 367:752–763.
17. Griesbeck O, Baird GS, Campbell RE, Zacharias DA, Tsien RY (2001) Reducing the environmental sensitivity of yellow fluorescent protein. *J Biol Chem* 276:29188–29194.
18. Wachter RM, Elsliger MA, Kallio K, Hanson GT, Remington SJ (1998) Structural basis of spectral shifts in the yellow-emission variants of green fluorescent protein. *Structure* 6:1267–1277.
19. Tsien RY (1998) The green fluorescent protein. *Annu Rev Biochem* 67: 509–544.
20. Verkhusha V, *et al.* (2003) Effect of high pressure and reversed micelles on the fluorescent proteins. *Biochim Biophys Acta* 1622:192–195.
21. Kim CU, Chen Y, Tate MW, Gruner SM (2008) Pressure-induced high-density amorphous ice in protein crystals. *J Appl Crystallogr* 41:1–7.
22. Frauenfelder H, *et al.* (1987) Thermal Expansion of a Protein. *Biochemistry* 26:254–261.
23. Hadfield A, Hajdu J (1993) A fast and portable microspectrophotometer for protein crystallography. *J Appl Crystallogr* 26:839–842.
24. Klink BU, Goody RS, Scheidig AJ (2006) A newly designed microspectrofluorometer for kinetic studies on protein crystals in combination with x-ray diffraction. *Biophys J* 91:981–992.
25. Kim CU, Hao Q, Gruner SM (2007) High-pressure cryocooling for capillary sample cryoprotection and diffraction phasing at long wavelengths. *Acta Crystallogr D* 63:653–659.
26. Cruickshank DWJ (1999) Remarks about protein structure precision. *Acta Crystallogr D* 55:583–601.
27. Kabsch W (1976) Solution for best rotation to relate 2 sets of vectors. *Acta Crystallogr A* 32:922–923.
28. Heremans K, Smeller L (1998) Protein structure and dynamics at high pressure. *Biochim Biophys Acta* 1386:353–370.
29. Dietz H, Rief M (2004) Exploring the energy landscape of GFP by single-molecule mechanical experiments. *Proc Natl Acad Sci USA* 101:16192–16197.
30. Dietz H, Rief M (2006) Protein structure by mechanical triangulation. *Proc Natl Acad Sci USA* 103:1244–1247.
31. Dietz H, Berkemeier F, Bertz M, Rief M (2006) Anisotropic deformation response of single protein molecules. *Proc Natl Acad Sci USA* 103:12724–12728.
32. Toniolo A, Granucci G, Martínez TJ (2003) Conical intersections in solution: A QM/MM study using floating occupation semiempirical configuration interaction wave functions. *J Phys Chem A* 107:3822–3830.
33. Sinicropi A, Andruniow T, Ferré N, Basosi R, Olivucci M (2005) Properties of the emitting state of the green fluorescent protein resolved at the CASPT2//CASSCF/CHARMM level. *J Am Chem Soc* 127:11534–11535.
34. DePristo M, Bakker PIW, Blundell TL (2004) Heterogeneity and inaccuracy in protein structures solved by x-ray crystallography. *Structure* 12:831–838.
35. Liu R, Baase W, Matthews BW (2000) The introduction of strain and its effects on the structure and stability of T4 lysozyme. *J Mol Biol* 295:127–145.
36. Rossmann MG, van Beek CG (1999) Data processing. *Acta Crystallogr D* 55:1631–1640.
37. Kabsch W (1988) Evaluation of single-crystal x-ray diffraction data from a position-sensitive detector. *J Appl Crystallogr* 21:916–924.
38. French S, Wilson K (1978) On the treatment of negative intensity observations. *Acta Crystallogr A* 34:517–525.
39. Vagin A, Teplyakov A (1997) MOLREP: An automated program for molecular replacement. *J Appl Crystallogr* 30:1022–1025.
40. Murshudov G, Vagin A, Dodson E (1997) Refinement of macromolecular structures by the maximum-likelihood method. *Acta Crystallogr D* 53:240–255.
41. Perrakis A, Morris RJ, Lamzin VS (1999) Automated protein model building combined with iterative structure refinement. *Nat Struct Biol* 6:458–463.
42. Emsley P, Cowtan K (2004) Coot: Model-building tools for molecular graphics. *Acta Crystallogr D* 60:2126–2132.
43. Laskowski R, MacArthur M, Moss D, Thornton JM (1993) PROCHECK: A program to check the stereochemical quality of protein structures. *J Appl Crystallogr* 26:283–291.

Supporting Information

Barstow *et al.* 10.1073/pnas.0802252105

SI Text

Expression and Crystallization. The gene for weakly dimeric citrine (1) (where residue 206 is an alanine) was kindly provided by R. Y. Tsien (University of California at San Diego) in a pRSETB plasmid (Invitrogen). To achieve higher expression and affinity tag digestion efficiency, the citrine plasmid was copied from the pRSETB plasmid by PCR, simultaneously replacing the EKMax (Invitrogen) protease cut site linking the protein and its polyhistidine affinity tag with a Tobacco Etch Virus (TEV) protease cut site. The new construct was then ligated into a pET28 vector (Novagen). The procedure resulted in a protein with an additional glycine residue at the N terminus when compared with the protein originally studied by Griesbeck *et al.* (1).

The plasmid was used to transform *Escherichia coli* strain BL21 (Invitrogen), grown for 24 h in a LB broth with kanamycin at 37°C, and induced with 100 mM IPTG. Protein overexpression was allowed to proceed for 6 h. The cell cultures were then spun at 14,000 × *g* for ≈30 min to pellet the cells and were resuspended in an alkaline lysis buffer. The cells were then lysed in a French Press style cell disruptor. The lysate was then spun at 20,000 × *g* at 4°C for ≈30 min to pellet the cellular debris. Uncoiled genomic DNA was precipitated from the supernatant by slowing stirring in polyethylenimine to a final concentration of 0.5% vol/vol.

The supernatant was then loaded onto a Ni-NTA affinity column (HisTrap HP, catalog number 17-5248-01, GE Healthcare) and washed with an increasing concentration of imidazole solution. The citrine was then eluted with a high concentration imidazole solution. The affinity tags were digested by TEV protease overnight at 4°C in a TEV reaction buffer. Undigested protein and cleaved his-tags were removed by washing the protein through a Ni-NTA column. The flow through, the digested citrine, was collected and finally purified by gel filtration chromatography. The final gel filtration step appears to be redundant, and its absence appears to have no impact on the crystallizability of the protein.

After the final purification step, the protein was concentrated to 20 mg/ml with a Pall centrifugal concentrator (catalog number OD010C37, Pall Separation Systems), and its buffer was simultaneously exchanged for 50 mM HEPES at pH 7.5. The protein concentration was checked by measuring the absorption of the protein at 514 nm with a Nanodrop ND-1000 absorption spectrophotometer. Because citrine does not cold denature, large aliquots of the protein may be slow-frozen and thawed. Fifty-microliter aliquots of citrine solution were frozen at −70°C for long-term storage. Citrine appears to keep quite well at 4°C for at least 2 years.

The protein was crystallized by using a crystallization screen around the conditions reported by Griesbeck *et al.* (1) (50 mM sodium acetate, 50 mM ammonium acetate, and 7% PEG 3400; pH 5.0 and temperature at 4°C) using hanging drop crystallization. Hanging drops were initially a mixture of 1 μl of well solution and 1 μl of 20 mg/ml citrine in 50 mM HEPES at pH 7.5. The droplets were mixed thoroughly by pipetting. A single spontaneously nucleated crystal was found by using this screen with 50 mM sodium acetate (for later experiments, we used catalog number 71183-250G, lot number 71183-250G, Fluka), 50 mM ammonium acetate (for later experiments, we used catalog number 431311-50G, lot number 11019JC, Sigma–Aldrich), and 9% PEG 3350 (catalog number HR2-591, lot numbers 259134 and 259147, Hampton Research), at pH 4.5. We believe that the choice of sodium and ammonium acetate does not affect the crystallization of citrine, although the choice of PEG may, explaining the difference in crystallization experience in Griesbeck *et al.* (1). To avoid dilution of the hanging droplets by evaporation from the crystallization wells, it was found that the crystallization trays must be packed in styrofoam containers, before storage, at 4°C. The first crystal appeared after 7 days.

Further crystals were grown by seeding of the single spontaneously nucleated crystal, using a 5% PEG 3350, 50 mM sodium acetate, 50 mM ammonium acetate, pH 5.0 precipitant solution, and a Seed Bead (catalog number HR2-320, Hampton Research). No more than 12 crystal wells were set up at a single time. Sixty microliters of precipitant and 60 μl of 10 mg/ml citrine in 50 mM HEPES (pH 7.5) were mixed in a Seed Bead, and then 10 μl of this mixture was dispensed onto the cap of the Seed Bead. A crystal of citrine was transferred to the cap, and the Seed Bead was then centrifuged in a centrifuge precooled to 4°C for 10 seconds to remove the droplet from the cap. The Seed Bead was then vortexed for approximately one-quarter of a second, making sure that the bead moved around inside the Seed Bead. The Seed Bead was then recentrifuged to pellet the solution and immediately transferred to ice. The seeding solution was then dispensed onto cover-slides in 10-μl droplets, and each slide sealed onto a well before proceeding to the next well. The Seed Bead was chilled on ice between dispensations, and the whole procedure lasted no longer than 5 min. The sealed wells were immediately transferred to a styrofoam box and refrigerated at 4°C. Crystals appeared overnight, and grew to ≈300 × 50 × 50 μm within a few days (Fig. S1).

At least three forms of citrine crystals will grow under these conditions: bricks with the most equal dimensions, plates with two long dimensions and a very thin third dimension, and rods with one long dimension and two very short dimensions. The plate form of the citrine crystal does not appear to diffract well and has imperfect symmetry, only indexing well in a P2 or P1 space-group. The rod crystals have not been tested.

X-Ray Diffraction. To investigate the structural origin of citrine's fluorescence shift, a high-pressure cryocooling technique described by Kim *et al.* (2) was used to prepare citrine crystals at cooling pressures ranging from 50 to 500 MPa. In this technique, a protein crystal is pressurized to a target pressure with helium gas and is then cooled to liquid nitrogen temperature (77 K), locking in any structural changes induced by the elevated pressure (3). The pressure may then be released, but the protein molecules that compose the crystal will remain in their pressurized state as long as the crystal's temperature remains well below the glass transition temperature of the protein-solvent mixture (4, 5). A consequence of this preparation method is that each structure at each pressure is from a different crystal, and that each structure is derived at cryogenic temperatures.

X-ray diffraction data were collected at Cornell High Energy Synchrotron Source (CHESS) macromolecular crystallography station F2 at an x-ray wavelength of 0.9795 Å (the selenium edge) and with a 0.1-mm x-ray collimator, by using a Quantum 210 CCD detector (Area Detector Systems). For datasets taken in April and November 2007, the detector used an upgraded computer for image processing.

Crystals were transferred by hand from a liquid nitrogen storage dewar to a cryogenic nitrogen stream at 100 K (Oxford Cryosystems). Care should be taken when performing the transfer as even slight warming of the sample will allow the pressure-induced deformations in the sample to relax and re-

lease the helium gas trapped in the crystal. Typically, 120–180 oscillation images were taken from each crystal, with an angular separation of 1°, a 1° oscillation angle, and exposure times ranging from 30 to 60 seconds. Full data collection details are shown in Table S1.

The diffraction data were indexed with Rossmann and van Beek's (6) Data Processing Suite algorithm, integrated with MOSFLM (7), scaled with Scala (8) and truncated with Truncate (9). Indexing quality indicators for each structure are shown in Table S2. Unit cell axes for each model are shown in Table S3.

Crystallographic Refinement. The crystallographic refinement process was standardized for all datasets by performing many refinement trials in which the refinement parameters were varied to find a globally good procedure that minimized the R_{Free} factor for the maximum number of structures. This large search was conducted by using the Feynman parallel computer cluster at CHESS.

The procedure that was found to be most satisfactory was similar to that suggested by Kleywegt and Jones (10). Each dataset was truncated at a resolution where the average signal-to-noise calculated by Scala ($<I>/<\sigma>$) was 3.0, minimizing the R_{Free} factor and minimizing the Log Likelihood Gain (LLG) (11) of the resulting model. For each structure, molecular replacement was performed by Molrep (12) in the space group $P2_12_12_1$, by using the 1HUY structure of Griesbeck *et al.* (1), stripped of solvent and with residue 80 mutated from an arginine to a glutamine as a search model.

Molecular replacement was followed by 10 cycles of rigid body refinement using refmac5 (11). Next, 10 cycles of restrained refinement with overall temperature factor refinement were performed by refmac5, followed by 10 cycles of restrained refinement with isotropic B-factor refinement for each atom. For all steps using refmac5, the maximum likelihood residual was used (11).

Finally, five cycles of solvent addition, followed by five cycles of restrained refinement with isotropic B-factor refinement, were performed using the ARP/wARP program by Perrakis *et al.* (13, 14) and refmac5, until the R_{Free} factor (15) and LLG function (11) were simultaneously minimized. The number of restrained refinement cycles in the final solvent addition-restrained refinement cycle was chosen to minimize R_{Free} and LLG. Finally, the structures were validated with Coot (16) and PROCHECK (17). The resolutions of the datasets ranged from 2.46 to 1.5 Å. Refinement quality indicators for each structure are shown in Table S4. PDB accession codes for the structures are shown in Table S5.

Room Temperature Spectroscopy. Room temperature, high-pressure spectra of citrine were measured by using an ISS high-pressure fluorescence cell and an ISS Chronos spectrophotometer. Temperature control of the sample was provided by water cooling the high-pressure cell using a Neslab (Thermo Scientific) water bath set to 25°C, with feedback provided by a thermocouple directly attached to the high-pressure cell. One-half-millimeter slits with a 4-nm bandwidth were used.

Solutions of citrine were prepared at a concentration of 0.0053 mg/ml, giving an absorbance of 0.1 over the 0.7-cm path length of the fluorescence cuvette. At this concentration, citrine is monomeric. Citrine was prepared in three buffers: 50 mM HEPES at pH 7.5; 50 mM Tris at pH 7.5 [a buffer known to be insensitive to high pressure (18, 19)]; and a precipitant solution, 50 mM sodium acetate, 50 mM ammonium acetate, and 5% wt/vol PEG 3350 at pH 5.0. The fluorescence spectrum of citrine in each of these solutions was measured over the pressure range 0.1–350 MPa. In each case, the fluorescence shift was linear with pressure. In both pH 7.5 buffers, the fluorescence shift was indistinguishable, with the peak of fluorescence shifting from 528.3 nm at ambient pressure by 0.912 nm per 100 MPa (per 1000 atmospheres). At pH 5.0, the fluorescence peak begins at 528.3 nm at ambient pressure, but shifts at a similar but slightly higher rate: 1.14 nm per 100 MPa. A plot of this behavior is shown in Fig. S2.

Low Temperature Spectroscopy. As the thermal contraction of a protein molecule between room temperature and 100 K is comparable with the changes because of pressurization (20), it was important to measure the fluorescence spectra of pressure-cooled samples to establish a direct link between structure of the molecule and its fluorescence properties.

We constructed a low-temperature fluorescence and absorption spectroscopy apparatus, drawing upon the designs of Hadfield (21) and Klink *et al.* (22). Like Hadfield's apparatus, the device has the ability to measure the absorption of small crystalline samples and, like that of Klink *et al.* (22), features backscattering fluorescence, allowing easy measurement of the fluorescence spectrum of a sample without the need to align the collection and excitation optics, because they are both the same combined in a single optic.

Fluorescence excitation was provided by a high stability 473-nm diode laser (catalog number LRS-473-TM-10, LaserGlow). The power output of the device was limited upon our request to 5 mW to ensure classification as a class IIIa laser, coupled by a bifurcated fiber optic bundle (Romack) to a long working length, high numerical aperture reflecting objective (catalog number NT58-417, Edmund Optics), and used for both excitation and collection optics in the fluorescence backscattering mode. The laser beam spectral width was narrowed by a train of band-pass optical interference filters; one high transmission 473-nm filter (catalog number LD01-473/10-12.5, Semrock), and two lower transmission filters at 470 (catalog number NT43-062, Edmund Optics) and 467 nm (catalog number NT43-061, Edmund Optics).

The backscattered fluorescence light was analyzed with an Ocean Optics USB2000 spectrophotometer with a 200-μm slit and a #2 grating. The spectrophotometer was calibrated before use by fiber connection to a blackbody calibration source (DH-2000 Calibration lamp*, Ocean Optics).

Because of the high optical density and overlapping absorption and fluorescence spectra of citrine crystals, we were unable to repeatedly measure the position of the peak of the fluorescence spectra of pressure-cooled citrine crystals because of small size variations in the crystals. Thus, we were forced to seek a substitute: pressure cryocooled solutions in capillaries.

Citrine stock solution (20 mg/ml citrine in 50 mM HEPES, pH 7.5) was slowly dialyzed into crystallization precipitant solution (5% PEG 3350, 50 mM sodium acetate, 50 mM ammonium acetate, pH 5.0) and diluted to 1 mg/ml. The solution was loaded into optically clear polycarbonate capillaries (plastic part number 8-000-1000, length 5 inches (127 mm), inner diameter 0.012 inches (304.8 μm), outer diameter 0.036 inches (914.4 μm), Drummond Scientific), cut to ≈18 mm in length so as to match the length of a mounted cryoloop, and frozen in the high-pressure cryocooling apparatus (23). The frozen capillaries were transferred inside a liquid nitrogen dewar to the crystal spectrophotometer and transferred by hand to the station's goniometer mount.

The sample was aligned to the excitation/collection optics by translations of the crystal station goniometer, viewing with a 40× telescope with a working distance of 1 inch (2.54 cm), using

*Ocean Optics sells a blackbody lamp and blackbody calibration source both called the DH-2000. We used the calibration version that has a carefully calibrated spectrum but much lower intensity.

a grid reticule (catalog number NT39,446, Edmund Optics) as a reference mark.

In addition to measuring the peak of high-pressure cryocooled citrine solutions as a function of temperature as described in the main text, the fluorescence peak of pressure cryocooled citrine crystals was also measured, and it was found that the peak of the crystal would remain approximately constant, as the temperature of the cold stream was raised, until it passed a critical transition temperature of the crystal. The peak would then rapidly shift to the yellow, suggesting that the citrine molecules had relaxed to their ambient pressure state, as was observed in high-pressure cryocooled solutions. Upon recooling, the fluorescence peak remained in a yellow-shifted state. A plot of this behavior for a citrine crystal cryocooled at 175 MPa is shown in Fig. S3.

1. Griesbeck O, Baird GS, Campbell RE, Zacharias DA, Tsien RY (2001) Reducing the environmental sensitivity of yellow fluorescent protein. *J Biol Chem* 276:29188–29194.
2. Kim CU, Kapfer R, Gruner SM (2005) High-pressure cooling of protein crystals without cryoprotectants. *Acta Crystallogr D* 61:881–890.
3. Urayama P, Phillips GN, Gruner SM (2002) Probing substates in sperm whale myoglobin using high-pressure crystallography. *Structure* 10:51–60.
4. Frauenfelder H, *et al.* (1990) Proteins and pressure. *J Phys Chem* 94:1024–1037.
5. Kim CU, Chen Y, Tate MW, Gruner SM (2008) Pressure-induced high-density amorphous ice in protein crystals. *J Appl Crystallogr* 41:1–7.
6. Rossmann MG, van Beek CG (1999) Data processing. *Acta Crystallogr D* 55:1631–1640.
7. Leslie AGW (1992) *Joint CCP4 + ESF-EAMCB Newsletter on Protein Crystallography* 26.
8. Kabsch W (1988) Evaluation of single-crystal x-ray diffraction data from a position-sensitive detector. *J Appl Crystallogr* 21:916–924.
9. French S, Wilson K (1978) On the treatment of negative intensity observations. *Acta Crystallogr A* 34:517–525.
10. Kleywegt GJ, Jones TA (1995) Braille for pugilists in *Making the Most of Your Model,* eds Hunter WN, Thornton JM, Bailey S (SERC Daresbury Laboratory, Warrington, UK), pp 11–24.
11. Murshudov G, Vagin A, Dodson E (1997) Refinement of macromolecular structures by the maximum-likelihood method. *Acta Crystallogr D* 53:240–255.
12. Vagin A, Teplyakov A (1997) MOLREP: An automated program for molecular replacement. *J Appl Crystallogr* 30:1022–1025.
13. Perrakis A, Morris RJ, Lamzin VS (1999) Automated protein model building combined with iterative structure refinement. *Nat Struct Biol* 6:458–463.
14. Morris RJ, Perrakis A, Lamzin VS (2003) ARP/wARP and automatic interpretation of protein electron density maps. *Methods Enzymol* 374:229–244.
15. Brünger AT (1992) Assessment of phase accuracy by cross validation: The free R value. Methods and applications. *Nature* 355:472–475.
16. Emsley P, Cowtan K (2004) Coot: Model-building tools for molecular graphics. *Acta Crystallogr* D60:2126–2132.
17. Laskowski R, MacArthur M, Moss D, Thornton JM (1993) PROCHECK: A program to check the stereochemical quality of protein structures. *J Appl Crystallogr* 26:283–291.
18. Zipp A, Kauzmann W (1973) Pressure denaturation of metmyoglobin. *Biochemistry* 12:4217–4228.
19. Neuman RC, Kauzmann W, Zipp A (1973) Pressure dependence of weak acid ionization in aqueous buffers. *J Phys Chem* 77:2687–2691.
20. Frauenfelder H, *et al.* (1987) Thermal Expansion of a protein. *Biochemistry* 26:254–261.
21. Hadfield A, Hajdu J (1993) A fast and portable microspectrophotometer for protein crystallography. *J Appl Crystallogr* 26:839–842.
22. Klink BU, Goody RS, Scheidig AJ (2006) A newly designed microspectrofluorometer for kinetic studies on protein crystals in combination with x-ray diffraction. *Biophys J* 91:981–992.
23. Kim CU, Hao Q, Gruner SM (2007) High-pressure cryocooling for capillary sample cryoprotection and diffraction phasing at long wavelengths. *Acta Crystallogr D* 63:653–659.

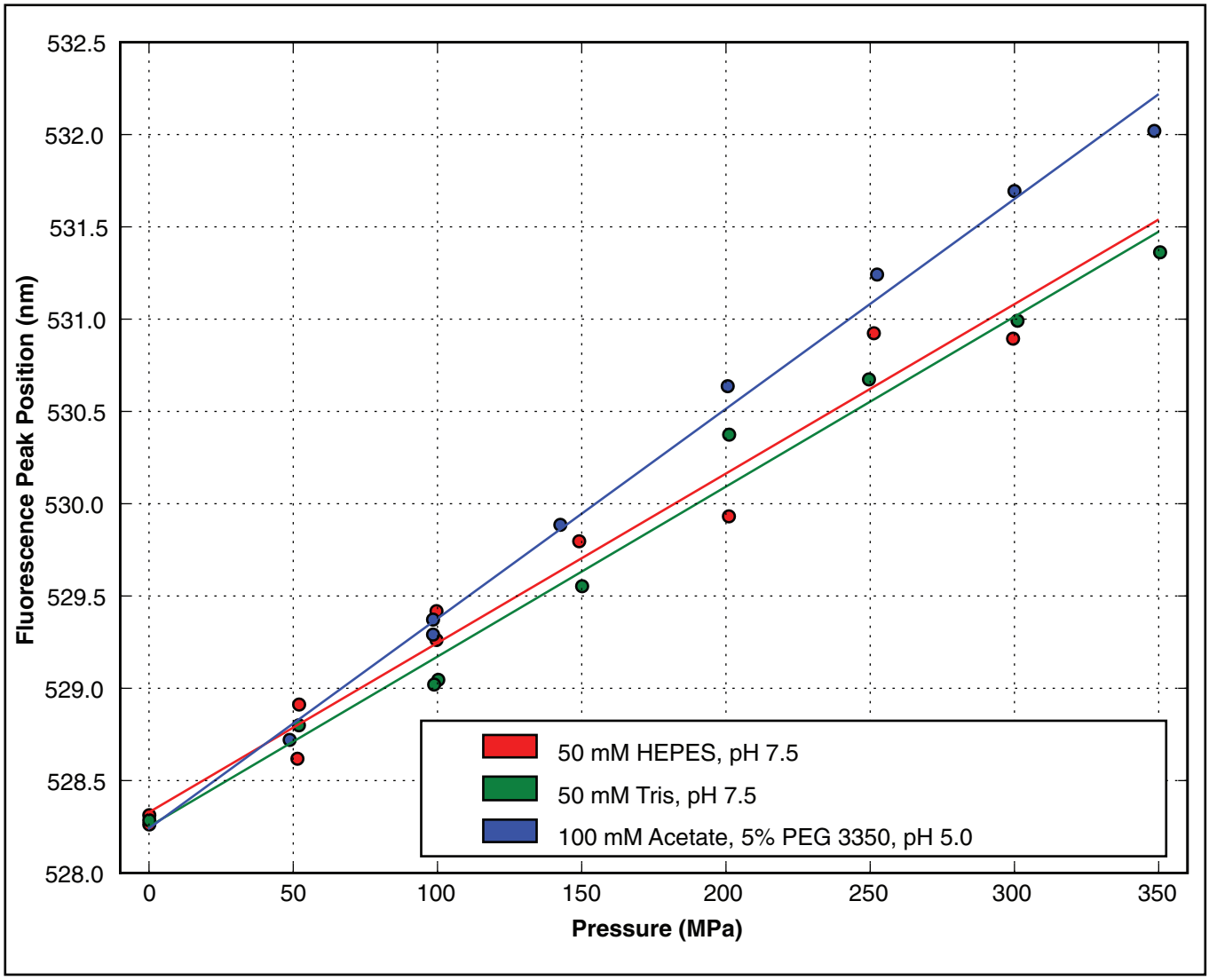

Fig. S1. Fluorescence peak shift of citrine in various buffers at room temperature.

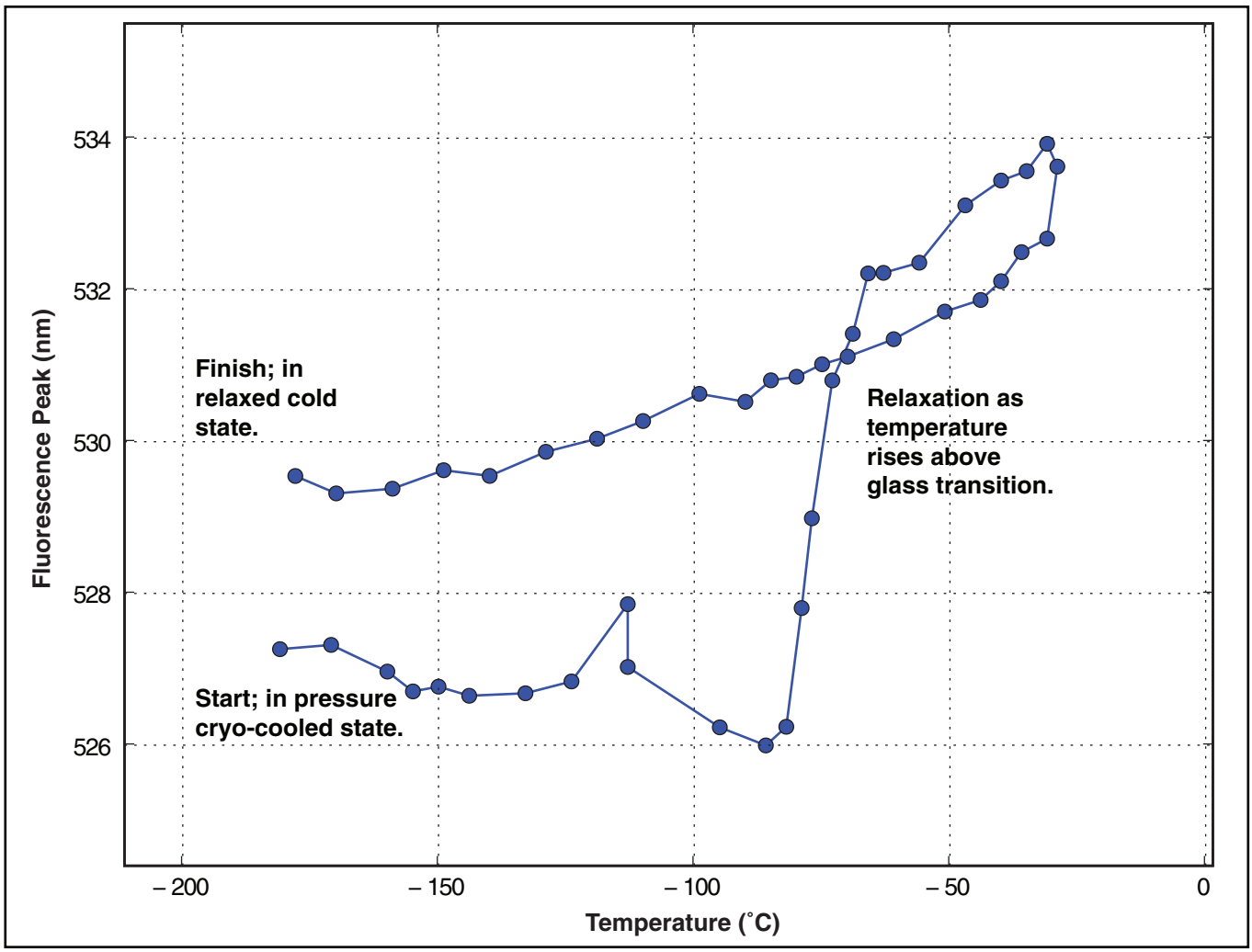

Fig. S2. Fluorescence peak of high pressure cooled citrine crystal as it is warmed and then recooled.

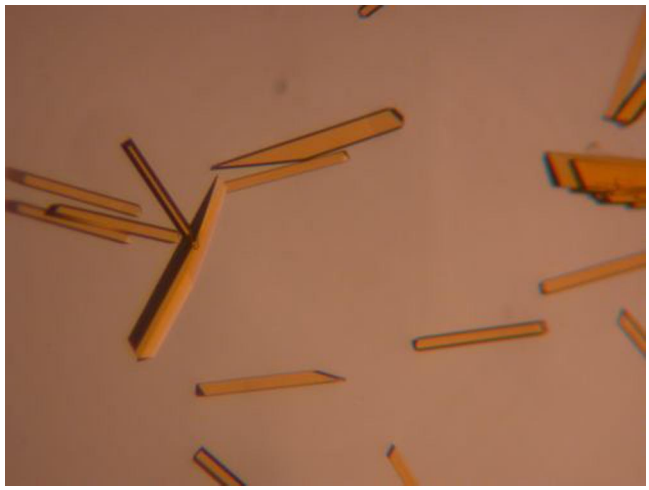

Fig. S3. Citrine crystals used in x-ray diffraction experiments.

Table S1. Crystallographic data collection information

Crystal	Pressure, MPa	Run	Distance, mm	Exposure time, s	Frames	Mosaicity, °
CitrineFF1	0.1	1	200.67	90	30	0.496
CitrineFF2	0.1	1	201.17	90	30	0.74
CitrineOFF2	0.1	1	200.42	25	120	0.538
Citrine0001_10	0.1	1	170.43	30	190	0.402
Citrine0500_1	50	1	199.35	60	120	0.527
Citrine0500_2	50	1	169.37	60	120	0.668
Citrine0500_3	50	1	194.7	30	180	0.546
Citrine0750_2	75	1	169.49	60	120	0.593
Citrine0750_4	75	1	194.71	60	120	1.038
Citrine1000_1	100	1	169.35	60	120	0.61
Citrine1000_2	100	1	169.3	60	120	0.551
Citrine1000_3	100	1	169.28	60	180	0.872
Citrine1000_5	100	1	194.89	30	180	0.912
Citrine1000_7	100	1	194.83	30	180	0.365
Citrine1000_8	100	1	195.35	30	105	0.524
Citrine1250_1	125	1	169.57	60	120	0.402
Citrine1250_2	125	1	169.09	60	120	0.912
Citrine1250_3	125	1	169.4	60	120	0.719
Citrine1250_4	125	1	179.89	25	200	0.672
Citrine1500_1	150	1	169.37	60	120	0.598
Citrine1500_2	150	1	169.3	60	120	0.843
CitrineOPF2	192	1	200.82	60	10	0.078
	192	2	160.84	60	7	0.113
	192	3	140.77	60	120	0.159
	192	4	140.71	60	120	0.125
CitrineOPF3	192	1	200.62	60	90	0.162
	192	2	199.66	60	90	0.086
Citrine1960_2	196	1	179.34	30	120	0.685
Citrine2000_2	200	1	195.05	30	120	0.566
	200	2	194.91	30	120	0.481
Citrine2000_3	200	1	194.95	60	151	0.44
	200	2	194.89	30	120	0.412
Citrine2500_1	250	1	197.71	20	120	0.291
Citrine4000_1	400	1	177.49	45	180	0.362
Citrine4000_2	400	1	177.67	30	180	0.904
Citrine4000_3	400	1	177.54	30	180	0.632
Citrine5000_3	500	1	167.75	30	180	0.554

All datasets were taken at Cornell High Energy Synchrotron Source macromolecular crystallography station F2 with a Quantum 210 CCD detector (Area Detector Systems). All datasets were taken by using a 0.1-mm X-ray collimator with an X-ray wavelength of 0.9795. Datasets Citrine0001_10 and Citrine2500_1 to Citrine5000_3 were taken after an upgrade to this detector. All datasets were taken with an oscillation angle of 1° and a step of 1°, except CitrineFF1 and CitrineFF2, which were taken with a 3° oscillation angle and step.

Table S2. Crystallographic indexing quality indicators for the datasets first shown in Table S1

Composite dataset	Pressure, MPa	R_{Merge}		R_{Meas}		Total Obs.		Unique Obs.		⟨I⟩/(σ)		Comp.		Mult.		
		OA	FS	OA	FS	OA	FS	OA	FS	OA	FS	OA	FS	OA	FS	Res, Å
CitrineFF1	0.1	0.078	0.247	0.091	0.291	49,882	6,947	14,127	2,015	13.8	5.2	99.6	99.9	3.5	3.4	2.07
CitrineOFF2	0.1	0.104	0.266	0.118	0.300	38,506	5,656	8,286	1,190	13.2	6.6	96.8	98.1	4.6	4.8	2.46
Citrine0001_10	0.1	0.072	0.253	0.078	0.276	156,833	19,104	21,406	2,994	21.0	6.1	98.8	96.2	7.3	6.4	1.80
Citrine0500_1	50	0.078	0.291	0.088	0.327	58,588	8,522	12,169	1,786	16.4	6.5	96.4	98.4	4.8	4.8	2.17
Citrine0500_2	50	0.062	0.339	0.070	0.380	92,045	13,407	19,193	2,737	20.1	4.8	97.9	96.6	4.8	4.9	1.87
Citrine0500_3	50	0.062	0.301	0.067	0.329	143,182	18,197	20,518	2,932	22.7	5.4	99.9	99.7	7.0	6.2	1.84
Citrine0750_2	75	0.056	0.300	0.063	0.337	99,597	14,165	20,832	3,034	19.3	4.3	98.6	99.7	4.8	4.7	1.82
Citrine0750_4	75	0.071	0.293	0.080	0.331	69,765	10,118	15,261	2,165	16.7	4.9	100.0	100.0	4.6	4.7	2.04
Citrine1000_1	100	0.072	0.287	0.081	0.322	79,351	11,489	16,780	2,412	17.8	5.0	99.3	99.9	4.7	4.8	1.97
Citrine1000_2	100	0.079	0.325	0.089	0.364	85,903	12,501	18,149	2,581	17.1	4.6	99.5	99.3	4.7	4.8	1.92
Citrine1000_3	100	0.087	0.273	0.094	0.295	107,660	15,551	15,568	2,219	20.9	6.1	100.0	100.0	6.9	7.0	2.03
Citrine1000_5	100	0.062	0.292	0.067	0.315	112,129	16,377	16,109	2,310	24.5	6.4	100.0	100.0	7.0	7.1	2.01
Citrine1000_7	100	0.058	0.271	0.063	0.307	165,929	11,813	25,494	2,831	22.8	4.0	94.9	73.9	6.5	4.2	1.67
Citrine1000_8	100	0.071	0.260	0.081	0.303	79,760	10,431	19,594	2,807	15.6	4.4	99.9	99.8	4.1	3.7	1.86
Citrine1250_1	125	0.061	0.306	0.069	0.343	97,386	14,128	20,246	2,933	18.4	4.7	98.9	99.9	4.8	4.8	1.84
Citrine1250_2	125	0.064	0.303	0.072	0.343	70,155	10,212	15,203	2,169	18.9	4.6	99.9	100.0	4.6	4.7	2.04
Citrine1250_3	125	0.066	0.287	0.074	0.320	72,130	10,386	15,091	2,178	18.3	5.1	98.3	99.5	4.8	4.8	2.04
Citrine1250_4	125	0.060	0.342	0.064	0.366	159,534	23,049	20,337	2,907	26.5	5.9	100.0	100.0	7.8	7.9	1.86
Citrine1500_1	150	0.050	0.124	0.056	0.139	71,483	10,441	14,686	2,145	23.3	11.1	97.0	986.0	4.9	4.9	1.78
Citrine1500_2	150	0.068	0.307	0.075	0.341	70,320	10,237	13,736	2,027	19.6	5.4	91.5	93.8	5.1	5.1	2.04
CitrineOPF2	192	0.090	0.236	0.097	0.255	228,033	32,119	30,481	4,414	23.9	5.4	99.9	100.0	7.5	7.3	1.58
CitrineOPF3	192	0.085	0.239	0.092	0.280	126,611	7,074	20,560	2,050	19.9	3.3	92.4	64.7	6.2	3.5	1.75
Citrine1960_2	196	0.051	0.294	0.058	0.334	93,837	12,557	20,204	2,875	21.2	5.2	99.9	99.4	4.6	4.4	1.86
Citrine2000_2	200	0.070	0.303	0.074	0.325	194,213	23,902	21,016	2,987	27.6	5.3	100.0	99.8	9.2	8.0	1.83
Citrine2000_3	200	0.094	0.300	0.099	0.315	186,809	27,088	17,459	2,488	25.4	6.9	100.0	100.0	10.7	10.9	1.95
Citrine2500_1	250	0.057	0.263	0.064	0.313	89,750	5,932	20,485	2,212	17.7	3.1	91.9	69.5	4.4	2.7	1.78
Citrine4000_1	400	0.068	0.276	0.074	0.302	144,633	18,401	20,822	2,963	21.4	5.7	99.8	99.4	6.9	6.2	1.82
Citrine4000_2	400	0.089	0.274	0.097	0.296	70,739	10,304	10,412	1,472	20.1	7.0	100.0	100.0	6.8	7.0	2.25
Citrine4000_3	400	0.069	0.259	0.076	0.280	104,036	15,283	15,772	2,254	22.2	7.3	100.0	99.9	6.6	6.8	2.02
Citrine5000_3	500	0.070	0.269	0.075	0.290	144,252	20,256	20,121	2,843	23.7	7.6	98.0	96.8	7.2	7.1	1.80

Indicators are given for the overall (OA) dataset and for the final resolution shell (FS) of the dataset. All datasets were indexed by using Rossmann and van Beek's Data Processing Suite algorithm and scaled by using the CCP4 program SCALA.

Table S3. Unit cell axes for all citrine models

Model name	a, Å	b, Å	c, Å
citrine0001_2	51.385	62.624	69.994
citrine0001_18	51.376	62.375	70.639
citrine0500_9	51.383	63.056	70.804
citrine0750_16	51.336	62.886	71.1
citrine1000_1	51.408	62.99	71.315
citrine1000_2	51.362	62.928	71.297
citrine1000_3	51.413	63.122	71.225
citrine1000_5	51.475	62.935	71.664
citrine1000_7	51.401	61.976	70.561
citrine1000_8	51.45	62.272	70.366
citrine1250_1	51.36	62.8	71.0
citrine1250_2	51.193	62.977	71.128
citrine1250_3	51.44	63.356	71.575
citrine1250_4	51.462	63.34	71.672
citrine1500_1	51.459	62.784	71.163
citrine1500_2	51.343	62.982	71.084
citrine1920_2	51.447	63.223	66.653
citrine1920_3	51.271	62.77	66.11
citrine1960_2	51.549	63.127	71.464
citrine2000_2	51.428	62.944	71.205
citrine2000_3	51.418	63.207	70.904
citrine2500_1	51.363	62.74	70.185
citrine4000_1	51.366	69.993	62.499
citrine4000_2	51.126	60.56	67.209
citrine4000_3	51.531	62.653	71.471
citrine5000_3	51.621	61.06	68.132

All models were indexed in space group $P2_12_12_1$ with unit cell angles $\alpha = \beta = \gamma = 90$ Å.

Table S4. Atomic model quality indicators for all Citrine models

Model Name	R Factor	R Free	FOM	LLG	rmsBOND, Å	rmsANGLE, °	rmsCHIRAL	ESU Based on Free R Value, Å	Solvent Addition Cycles	Datasets Used
Citrine0001_2	0.205	0.31	0.74	46133.8	0.047	3.43	0.216	0.376	1+1	CitrineOFF2
Citrine0001_18	0.192	0.248	0.841	103613	0.017	1.805	0.099	0.154	48	Citrine0001_10
Citrine0500_9	0.18	0.235	0.851	93779.2	0.021	1.951	0.11	0.156	23+1	Citrine0500_1, Citrine0500_2
Citrine0750_16	0.181	0.26	0.826	59344.5	0.034	2.591	0.154	0.26	27+3	Citrine0750_2, Citrine0750_4
Citrine1000_1	0.188	0.251	0.821	85682.2	0.025	2.112	0.125	0.179	40+1	Citrine1000_1
Citrine1000_2	0.189	0.243	0.84	91087.4	0.023	2.039	0.122	0.164	33+1	Citrine1000_2
Citrine1000_3	0.19	0.261	0.813	80029.3	0.029	2.224	0.131	0.198	58+1	Citrine1000_3
Citrine1000_5	0.182	0.237	0.841	80258.1	0.026	2.119	0.122	0.176	57+4	Citrine1000_5
Citrine1000_7	0.182	0.232	0.858	124318.6	0.013	1.738	0.1	0.119	37+2	Citrine1000_7
Citrine1000_8	0.176	0.227	0.86	97333.4	0.019	1.919	0.113	0.146	59+1	Citrine1000_8
Citrine1250_1	0.188	0.262	0.84	100123	0.019	1.921	0.11	0.161	22	Citrine1250_1
Citrine1250_2	0.187	0.246	0.83	76717.5	0.027	2.28	0.136	0.19	46+1	Citrine1250_2
Citrine1250_3	0.189	0.265	0.808	76547.4	0.029	2.334	0.134	0.204	16+1	Citrine1250_3
Citrine1250_4	0.192	0.237	0.851	98702.4	0.02	1.952	0.112	0.147	22+4	Citrine1250_4
Citrine1500_1	0.196	0.23	0.857	105345.9	0.02	1.92	0.107	0.131	33+1	Citrine1500_1
Citrine1500_2	0.193	0.262	0.818	69944.7	0.028	2.333	0.132	0.21	14+2	Citrine1500_2
Citrine1920_2	0.198	0.236	0.857	143356.6	0.014	1.673	0.093	0.102	28+1	CitrineOPF2
Citrine1920_3	0.191	0.253	0.841	101831.3	0.017	1.822	0.104	0.147	57+1	CitrineOPF3
Citrine1960_2	0.197	0.249	0.828	98567.2	0.023	2.119	0.121	0.152	59+1	Citrine1960_2
Citrine2000_2	0.194	0.239	0.847	102853.4	0.021	1.99	0.114	0.143	44+1	Citrine2000_2
Citrine2000_3	0.182	0.239	0.85	87929	0.021	1.945	0.121	0.167	26+1	Citrine2000_3
Citrine2500_1	0.191	0.232	0.843	101124.2	0.018	1.855	0.102	0.137	29+1	Citrine2500_1
Citrine4000_1	0.215	0.266	0.826	106319.1	0.018	1.862	0.107	0.159	20+1	Citrine4000_1
Citrine4000_2	0.195	0.302	0.776	57520.8	0.041	2.95	0.169	0.305	18	Citrine4000_2
Citrine4000_3	0.196	0.264	0.826	81240.7	0.026	2.13	0.118	0.199	34+1	Citrine4000_3
Citrine5000_3	0.177	0.242	0.845	103711.9	0.018	1.835	0.105	0.149	59	Citrine5000_3

In the final column, where solvent addition cycles are denoted as $x + y$, x refers to the number of complete solvent addition and refinement cycles, and y refers to the number of refinement cycles in the final step.

Table S5. PDB accession codes for high-pressure Citrine structures

Model Name	PDB Code	RCSB Code
Citrine0001_2	3DPW	RCSB048340
Citrine0001_18	3DQO	RCSB048368
Citrine0500_9	3DQN	RCSB048367
Citrine0750_16	3DQM	RCSB048366
Citrine1000_1	3DQL	RCSB048365
Citrine1000_2	3DQK	RCSB048364
Citrine1000_3	3DQJ	RCSB048363
Citrine1000_5	3DQI	RCSB048362
Citrine1000_7	3DQH	RCSB048361
Citrine1000_8	3DQF	RCSB048359
Citrine1250_1	3DQE	RCSB048358
Citrine1250_2	3DQD	RCSB048357
Citrine1250_3	3DQC	RCSB048356
Citrine1250_4	3DQA	RCSB048354
Citrine1500_1	3DQ9	RCSB048353
Citrine1500_2	3DQ8	RCSB048352
Citrine1920_2	3DQ7	RCSB048351
Citrine1920_3	3DQ6	RCSB048350
Citrine1960_2	3DQ5	RCSB048349
Citrine2000_2	3DQU	RCSB048374
Citrine2000_3	3DQ4	RCSB048348
Citrine2500_1	3DQ3	RCSB048347
Citrine4000_1	3DQ2	RCSB048346
Citrine4000_2	3DQ1	RCSB048345
Citrine4000_3	3DPZ	RCSB048343
Citrine5000_3	3DPX	RCSB048341